Chinese Chemical Letters 35 (2024) 109789

Contents lists available at ScienceDirect

Chinese Chemical Letters

journal homepage: www.elsevier.com/locate/cclet

Constructing built-in electric field *via* CuO/NiO heterojunction for electrocatalytic reduction of nitrate at low concentrations to ammonia

Ying Chen[a,b,1], Xingyuan Xia[b,1], Lei Tian[b], Mengying Yin[b], Ling-Ling Zheng[a,b], Qian Fu[a,b], Daishe Wu[a,c,*], Jian-Ping Zou[a,b,*]

[a] Key Laboratory of Poyang Lake Environment and Resource Utilization, Ministry of Education, School of Resources & Environment, Nanchang University, Nanchang 330031, China
[b] National-Local Joint Engineering Research Center of Heavy Metals Pollutants Control and Resource Utilization, School of Environmental and Chemical Engineering, Nanchang Hangkong University, Nanchang 330063, China
[c] School of Materials and Chemical Engineering, Pingxiang University, Pingxiang 337000, China

ARTICLE INFO

Article history:
Received 24 January 2024
Revised 16 March 2024
Accepted 18 March 2024
Available online 19 March 2024

Keywords:
Electrocatalytic reduction of NO_3^--NH_4^+ selectivity
Built-in electric field
H^*
Low concentrations

ABSTRACT

Electrocatalytic reduction of nitrate (NO_3^-) at low concentrations to ammonia (NH_4^+) still faces challenges of low NO_3^- conversion and NH_4^+ selectivity due to the sluggish mass transfer and insufficient atomic hydrogen (H^*) supply. Herein, we propose CuO/NiO heterojunction with the assistance of a built-in electric field to enhance mass transfer and H^* provision. The built-in electric field in CuO/NiO is successfully formed as demonstrated by X-ray photoelectron spectroscopy and ultraviolet photoemission spectroscopy. The results reveal that CuO/NiO achieves high NO_3^- reduction activity (100%) and NH_4^+ selectivity (100%) under low NO_3^- concentration conditions (100 mg/L NO_3^-, *ca.* 22.6 mg/L NO_3^--N), which is superior to that of many recently reported electrocatalysts. Density functional theory calculations further clarify that the built-in electric field triggers the enhanced adsorption of reactants on CuO/NiO heterojunction interface and strong d-p orbital hybridization between reactants and CuO/NiO. Besides, the free energy diagram of hydrogen evolution reaction of CuO/NiO confirms the realization of enhanced H^* provision. Moreover, coupling experiments and consecutive cycle tests demonstrate the potential of CuO/NiO in practical applications. This work may open up a new path and guide the development of efficient electrocatalysts for electrocatalytic reduction of NO_3^- at low concentrations to NH_4^+.

The widespread nitrate (NO_3^-) pollution in water environment seriously endangers human health and environmental safety [1,2]. Electrocatalytic reduction of NO_3^- to industrially valuable ammonia (NRA) has been recognized as a "two birds with one stone" strategy to alleviate nitrate pollution and restore nitrogen cycle [3]. Recently, Cu-based catalysts have been found to be effective for electrocatalytic NRA due to their favorable NO_3^--binding ability [4]. However, the residual NO_3^- after electroreduction treatment of nitrate-contaminated water by the reported Cu-based catalysts does not meet the drinking water standard [5]. In practice, the NO_3^- concentration in many polluted waters (such as industrial wastewater and groundwater) is typically low [2,6]. Therefore, it is essential to develop Cu-based catalysts with high activity and selectivity for electrocatalytic reduction of NO_3^- at low concentrations to NH_4^+.

There are two crucial bottlenecks for Cu-based catalysts to achieve efficient electrocatalytic reduction of NO_3^- at low concentrations to NH_4^+: i) The small concentration gradients of reactants (*i.e.,* NO_3^- and its reaction intermediates) near electrocatalyst surface region leads to sluggish mass transfer [5,7]; ii) the sluggish Volmer step (H_2O-to-H^*) on Cu-based catalysts leads to the insufficient supply of atomic hydrogen (H^*) [2,8]. Therefore, enhancing mass transfer of reactants and H^* provision is the key to the design of Cu-based catalysts for electrocatalytic reduction of NO_3^- at low concentrations to NH_4^+. Currently, defect engineering has been employed to regulate the electron-density distribution and surface properties of Cu-based catalysts, thereby strengthening the adsorption of reactants and H^* [1,9]. Unfortunately, the occurrence of defects in Cu-based catalysts is mostly random and uncontrollable, which inevitably brings about the uncontrollable NO_3^- electroreduction pathway [10]. Thus, the controllable modification of Cu-based catalysts is advantageous for achieving high-efficiency electrocatalytic reduction of NO_3^- at low concentrations to NH_4^+.

* Corresponding authors.
E-mail addresses: dswu@ncu.edu.cn (D. Wu), zjp_112@126.com (J.-P. Zou).
[1] These authors contributed equally to this work.

https://doi.org/10.1016/j.cclet.2024.109789
1001-8417/

Recent works demonstrate that heterostructure design is an attractive approach for the controllable modification of Cu-based catalysts [11–13]. When Cu-based catalyst and other semiconductor with different work functions (Φ) contact to form a heterojunction, the built-in electric field is spontaneously generated in the interface region, thereby accelerating electronic transfer at the interface [14–17]. This can lead to local charge polarization and asymmetrical charge distribution in the interface region, significantly enhancing the adsorption of reactants [18]. Hence constructing a built-in electric field *via* Cu-based heterojunction is expected to enhance the mass transfer of low concentration reactants during electrocatalytic NRA process. In a similar consideration, Sun *et al.* [7] reported that the built-in electric field formed between CuCl and TiO_2 could effectively accumulate a higher concentration of NO_3^- near electrocatalyst surface region. Unfortunately, the high NO_3^- conversion and NH_4^+ selectivity are difficult to realize. The phenomenon is because the key problem of the insufficient H* supply is still ignored. As a result, the other semiconductor in the Cu-based heterojunction is required to enhance H* provision, thus guaranteeing the efficient electrocatalytic reduction of NO_3^- at low concentrations to NH_4^+.

In this work, inspired by nickel-based semiconductors with the superiority of H_2O-to-H* [19,20], we choose CuO and NiO with different work functions to form a heterojunction. A built-in electric field formed between CuO and NiO was confirmed by X-ray photoelectron spectroscopy and ultraviolet photoemission spectroscopy. The electrocatalytic NRA performance of CuO/NiO under low NO_3^- concentration conditions, including NO_3^- conversion, the selectivity of products (*i.e.,* NH_4^+, nitrite (NO_2^-), and dinitrogen (N_2)), and FE, was evaluated and compared with those of pure CuO and NiO. Impacts of reaction potential, solution pH, and NO_3^- concentration on electrocatalytic NRA performance of CuO/NiO were also investigated. Density functional theory (DFT) calculations revealed that CuO/NiO with a built-in electric field is advantageous for enhancing mass transfer of reactants and H* provision. Moreover, combining CuO/NiO system and electrochlorination could effectively induce NO_3^- to N_2 *via* a NO_3^--NH_4^+-N_2 route. The electrocatalytic stability of CuO/NiO was evaluated by consecutive cycle tests. The findings offer helpful guidance for the development and application of electrocatalytic NRA process for nitrate remediation with low concentration.

A two-step hydrothermal and calcination method was developed to synthesize CuO/NiO, as shown in Fig. S1 (Supporting information, and details in Experiment Section). The crystalline structures of the as-obtained catalyst were determined by X-ray diffraction (XRD). As shown in Fig. 1a, the diffraction peaks at 32.51°, 35.42°, and 38.90° correspond to the (110), (002), and (200) planes of CuO (JCPDS No. 48–1548), while the peaks at 37.25°, 43.29°, 62.88°, and 75.41° are assigned to the (111), (200), (220) and (311) planes of NiO (JCPDS No. 78–0429). The field-emission scanning

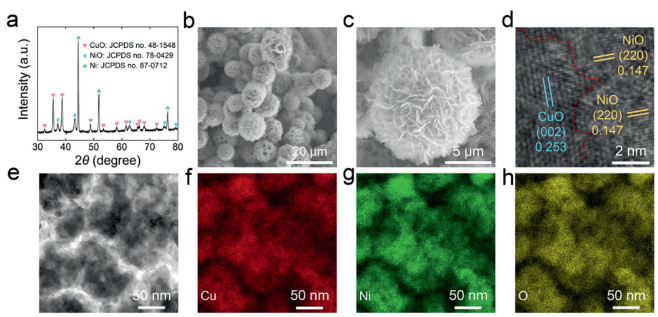

Fig. 1. (a) XRD pattern, (b, c) SEM imagines, (d) HRTEM image, (e–h) TEM elemental mapping images of CuO/NiO.

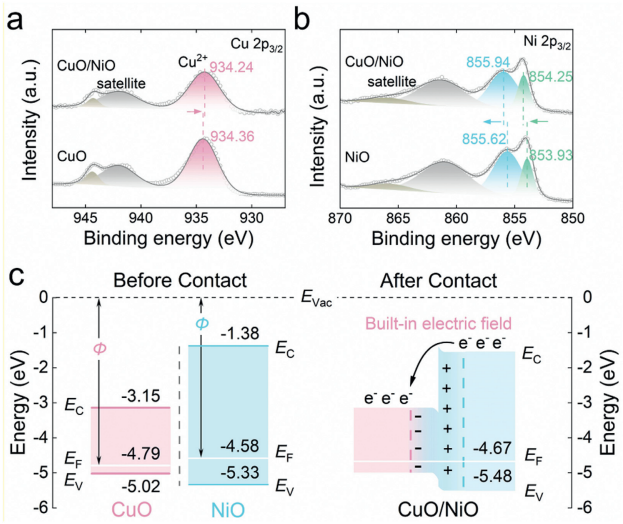

Fig. 2. (a) Cu $2p_{3/2}$ XPS spectra of CuO and CuO/NiO. (b) Ni $2p_{3/2}$ XPS spectra of NiO and CuO/NiO. (c) Band structures of CuO and NiO before contact (left) and energy band diagram of CuO/NiO (right).

electron microscopy (SEM) images unveil that the as-obtained catalyst has a flower-like microsphere structure (Figs. 1b and c). The phenomenon is due to the assistance of urea and ammonium fluoride in the hydrothermal process, which is consistent with the reported studies [21]. The high-resolution transmission electron microscopy (HRTEM) image reveals distinct lattice fringes with the lattice distance of 0.253 nm and 0.147 nm, which match well with that of the (002) plane of CuO and (220) plane of NiO, respectively (Fig. 1d). Besides, the corresponding elemental mapping results exhibit that Cu, Ni, and O are uniformly distributed in the flower-like microspheres (Figs. 1e–h). The above analysis confirms the successful synthesis of CuO/NiO *via* a facile hydrothermal and calcination method.

X-ray photoelectron spectroscopy (XPS) was employed to further unveil the chemical state of CuO/NiO. The Cu $2p_{3/2}$ spectrum consists of two satellite peaks and the characteristic peak of Cu^{2+} (934.24 eV) (Fig. 2a). Note that the characteristic Cu^{2+} peak of CuO/NiO shows a slight negative shift relative to that of pure CuO (934.36 eV). For Ni $2p_{3/2}$ spectrum, in addition to two satellite peaks, the peaks at 854.25 eV and 855.94 eV correspond to Ni^{2+} and Ni^{3+}, respectively (Fig. 2b). Besides, the Ni $2p_{3/2}$ spectrum displays that the characteristic peaks of Ni^{2+} and Ni^{3+} in CuO/NiO have an obvious positive shift of 0.32 eV compared to those of pure NiO. These findings manifest that the electron transfer exists from NiO to CuO in CuO/NiO. To further determine the electronic interaction between CuO and NiO, ultraviolet photoemission spectroscopy (UPS) was performed. As shown in Figs. S2a and b (Supporting information), the work function values of CuO and NiO are quantified to be 4.79 eV and 4.58 eV, respectively. The difference in work function ($\Delta\Phi$) between CuO and NiO begets a driving force for electron transfer, directing electron flow spontaneously from NiO to CuO. Moreover, the Fermi level (E_F) of CuO/NiO (−4.67 eV) is between E_F of CuO (−4.79 eV) and E_F of NiO (−4.58 eV), further testifying that the establishment of a built-in electric field in CuO/NiO (Figs. S2c in Supporting information). Furthermore, the valence band (E_V) values of CuO, NiO, and CuO/NiO heterojunction are measured to be −5.02 eV, −5.33 eV, and −5.48 eV by UPS spectra, respectively. Based on the above results and the energy gap (E_g) of CuO (1.87 eV) and NiO (3.95 eV) obtained in the reported studies [22], the energy band diagram of CuO/NiO is constructed in Fig. 2c. When CuO and NiO contact, the self-driven electron donation from NiO to CuO induces the energy band bending of both,

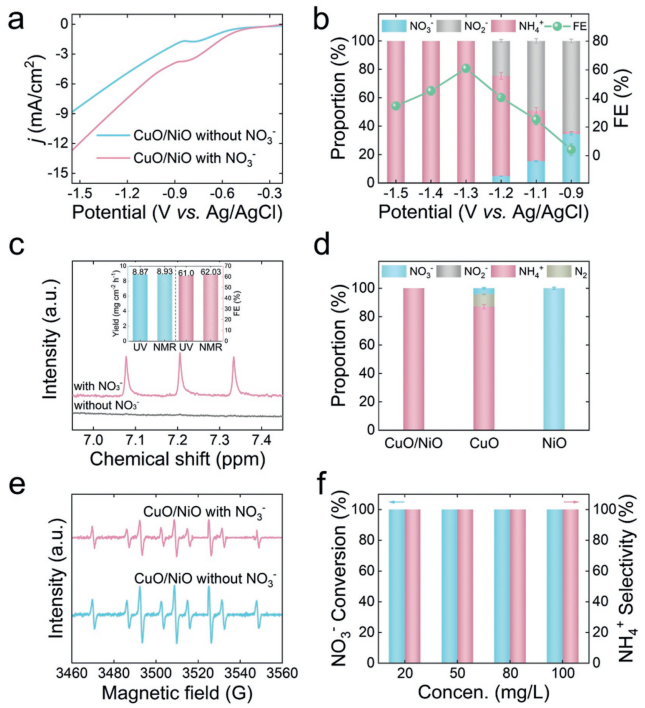

Fig. 3. (a) LSV curves of CuO/NiO in 0.05 mol/L Na_2SO_4 with and without 100 mg/L NO_3^-. (b) Product distribution of electrocatalytic NO_3^- reduction by CuO/NiO at different potentials. (c) ^1H NMR spectra of the electrolyte (0.05 mol/L Na_2SO_4 with and without 100 mg/L NO_3^-) after the electrocatalytic NRA reaction. Inset of (c): the quantitative comparison of the NH_4^+ yield rates and FEs achieved by CuO/NiO based on the NMR and UV–vis spectrophotometric methods. (d) Comparison of product distribution of electrocatalytic NO_3^- reduction by CuO/NiO, CuO, and NiO. (e) Dimethyl-1-pyrroline-*N*-oxide spin-trapping ESR spectra of H* stemmed from CuO/NiO in the absence and presence of NO_3^-. (f) Effect of initial NO_3^- concentration on NO_3^- conversion and NH_4^+ selectivity of CuO/NiO.

thus forming a built-in electric field at the heterojunction interface to accelerate charge transfer, thus accelerating electrocatalytic process [23,24].

The electrocatalytic NRA performance of CuO/NiO was assessed at room temperature using 0.05 mol/L Na_2SO_4 and low concentration NO_3^- (100 mg/L NO_3^-, *ca.* 22.6 mg/L NO_3^--N) as the electrolyte. To preliminarily investigate the electrocatalytic activity of CuO/NiO, linear sweep voltammetry (LSV) tests were conducted with or without the addition of NO_3^-. As shown in Fig. 3a, the addition of NO_3^- leads to a noticeable increase in the reduction current density of CuO/NiO, implying that NO_3^- can be reduced by CuO/NiO [25–27]. The concentrations of NO_3^-, NO_2^-, and NH_4^+ were determined by UV–vis spectrophotometric method and quantified by the corresponding standard curves (Fig. S3 in Supporting information). Fig. 3b displays that NO_3^- conversion increases from 65.5% at −0.9 V to 100% (*i.e.,* 8.87 NH_4^+-N mg cm^{-2} h^{-1}) at −1.3 V, and then maintains the maximum value of 100% in the potential range of −1.3 to −1.5 V. The NH_4^+ selectivity increases with increasing negative potential from −0.9 to −1.3 V and reaches 100% in the potential range of −1.3 to −1.5 V. NH_4^+ is not detected in a 0.05 mol/L Na_2SO_4 electrolyte without NO_3^- by nuclear magnetic resonance (NMR) and UV–vis spectrophotometric methods (Fig. 3c and Fig. S4 in Supporting information). These results exclude the possible interference of trace ammonia from air or other contaminants and confirm the origin of NH_4^+ *via* electrocatalytic NO_3^- reduction [28,29]. It is worthwhile to point out that CuO/NiO exhibits superior NO_3^- conversion efficiency and NH_4^+ selectivity efficiency than many recently reported electrocatalysts (such as FeSAs/g-C_3N_4, CuCl/TiO_2, Ag/GO/Ti, and Cu-SAC) under low NO_3^- concentration conditions (Table S1 in Supporting information). In addition, the corresponding FE of electrocatalytic NRA follows a volcano plot with the reaction potential. Specifically, the FE of NRA is as low as 4.3% at −0.9 V, and then gradually increases to the maximum value of 61.0% (at −1.3 V) with the increase of negative potential. This trend negatively correlates with the gradual decrease in the NO_2^- selectivity, demonstrating that NO_2^- is the intermediate product of electrocatalytic NRA process and can be further reduced to NH_4^+ at larger negative potentials. This is supported by the concentration-time curves of NO_3^--N, NO_2^--N, and NH_4^+-N at −1.3 V. With increasing reaction time, NO_3^--N concentration gradually decreases, NO_2^--N concentration follows a volcano-type trend, and NH_4^+-N concentration gradually increases (Fig. S5 in Supporting information). NMR was carried out to further determine the NH_4^+-yield and FE at −1.3 V. ^1H NMR spectra of different NH_4^+-concentrations were shown in Fig. S5a (Supporting information). By plotting the integral area of NH_4^+ peaks against the concentration, the standard curve was obtained (Fig. S5b in Supporting information). As shown in Fig. 3c, the concentration of NH_4^+ and FE calculated by the ^1H NMR spectroscopy and UV–vis spectrophotometric methods are nearly equal, evidently proving the accuracy of the two quantitative methods. In the potential range of −1.3 to −1.5 V, FE of NRA exhibits a decrease (34.8% – 45.3%), whereas NO_3^- conversion and NH_4^+ selectivity both remain unchanged (100%). The phenomenon could be attributed to the enhanced presence of competitive hydrogen evolution reaction at larger negative potentials [28]. Compared with some other electrocatalysts including CuCl/TiO_2 (44.7% FE, 100 mg/L NO_3^-) [5], single-atom iron (~50% FE, 20 mg/L NO_3^--N) [30], CuO/NiO exhibits higher FE (61.0%, 100 mg/L NO_3^-) for electrocatalytic reduction of NO_3^- at ultralow concentrations to NH_4^+ (Table S1). Considering that NO_3^- conversion, NH_4^+ selectivity, and FE are the important indexes of electrocatalytic NRA process, the applied potential at −1.3 V is chosen as the performing condition in the following experiments.

To determine the effect of the built-in electric field in CuO/NiO on electrocatalytic NRA performance, contrast experiments with pure CuO and NiO as catalysts for electrocatalytic NRA were carried out. As shown in Fig. 3d, CuO exhibits lower NO_3^- conversion (95.7%) and NH_4^+ selectivity (87.0%) than those of CuO/NiO. Moreover, the accumulation of N_2 might be due to the insufficient H* supply of CuO [31]. In addition, pure NiO has no effect on NO_3^- electroreduction, which might be altered for several reasons, such as superior HER activity, and too weak adsorption of low concentration NO_3^- [22,32]. These results affirm that the built-in electric field formed between CuO and NiO facilitates electrocatalytic reduction of NO_3^- at low concentrations to NH_4^+. To further understand the intrinsic performance of CuO/NiO, the electrochemically active surface areas (ECSA) of these catalysts were evaluated by electrochemical double-layer capacitance (C_{dl}) method. As shown in Fig. S6 (Supporting information), the C_{dl} value of CuO/NiO heterojunction (0.87 mF/cm) is higher than that of CuO (0.47 mF/cm) and NiO (0.85 mF/cm). The result highlights the built-in electric field at CuO/NiO can augment ECSA and expose more active sites, thereby promoting electrocatalytic NRA process [33,34].

To further elucidate the reaction mechanism in the CuO/NiO–mediated electrocatalytic NRA process, electron spin resonance (ESR) with the assistance of dimethyl-1-pyrroline-*N*-oxide (DMPO) as the radical trapping reagent was conducted to detect the existence of H* [35]. Nine typical signals with intensity ratios of 1:1:2:1:2:1:2:1:1 associated with DMPO-H* are observed in the spectrum of CuO/NiO without adding NO_3^- (Fig. 3e). The signal intensity of DMPO-H* decreases when NO_3^- is added, indicating that the generated H* is consumed in the electrocatalytic NRA process. Moreover, H* quenching experiment using tertiary butanol (TBA) was further performed [36]. The amount of residual NO_3^- increases with increasing TBA dosage, also suggesting that H* par-

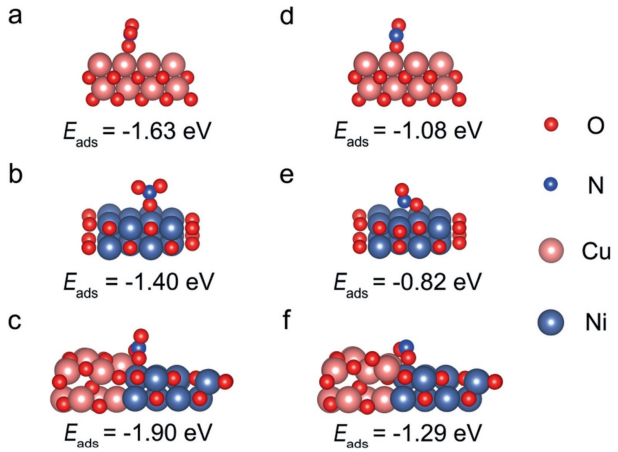

Fig. 4. Calculated adsorption energies of NO_3^- and NO_2^- on (a, d) CuO, (b, e) NiO, and (c, f) CuO/NiO.

ticipates in the electrocatalytic NRA process (Fig. S7 in Supporting information). Furthermore, CuO/NiO demonstrates remarkable NO_3^- conversion (>95%) and NH_4^+-N selectivity (>98%) in the pH range of 4–10 (Fig. S8 in Supporting information). The observation may be because CuO/NiO affords the built-in electric field for the enhanced adsorption of reactants, thereby weakening the influence of initial pH change on electrocatalytic NRA process. In addition, Fig. 3f shows that CuO/NiO can achieve NO_3^- conversion of 100% and NH_4^+ selectivity of 100% regardless of NO_3^- concentration (20–100 mg/L NO_3^-). The result further proves that CuO/NiO with the assistance of a built-in electric field can guarantee the efficient mass transfer of low concentration reactants during electrocatalytic NRA process. All of these results provide experimental evidence to support the aforementioned electrocatalytic NRA mechanism of CuO/NiO.

The DFT calculations are performed to validate the built-in electric field formed between CuO and NiO in terms of enhanced mass transfer of reactants. It is well known that NO_3^- adsorption is the first and most important step for electrocatalytic reduction of NO_3^- at low concentrations to NH_4^+ [37]. As shown in Figs. 4a-c, the calculated adsorption energy of NO_3^- on CuO/NiO heterojunction interface is −1.90 eV, which is much higher than that on pure CuO (−1.63 eV) and NiO (−1.40 eV). Considering that electrocatalytic NRA involves the tandem process of NO_3^- to NO_2^- and NO_2^- to NH_4^+, the adsorption of NO_2^- intermediate is a decisive step for NH_4^+ generation in electrocatalytic reduction of NO_3^- at low concentrations to NH_4^+. As shown in Figs. 4d-f, the calculated adsorption energy of NO_2^- on CuO/NiO heterojunction interface is −1.29 eV, which is much higher than that on pure CuO (−1.08 eV) and NiO (−0.82 eV). These results affirm that the built-in electric field formed between CuO and NiO can enhance the adsorption of reactants (NO_3^- and NO_2^-), contributing to a higher coverage of reactants on the electrocatalyst surface region.

In addition, projected partial density of states (PDOS) is performed to further verify and support the above discussion. It is observed that the energy difference (ΔE) between d band center (ε_d) of CuO/NiO and p band center (ε_p) of NO_3^- is identified to be 2.61 eV, which is lower than ΔE between ε_p of NO_3^- and ε_d of CuO (2.85 eV) or ε_d of NiO (3.13 eV) (Figs. 5a-c). These results confirm that the strong interaction between CuO/NiO and NO_3^- originates from the strong d-p orbital hybridization between CuO/NiO and NO_3^- [38,39]. Figs. 5d-f show that the hybridization between CuO/NiO and NO_2^- is also stronger than that between NO_2^- and CuO or NiO. The above calculations confirm that the built-in electric field formed between CuO and NiO indeed achieves the enhanced mass transfer of reactants.

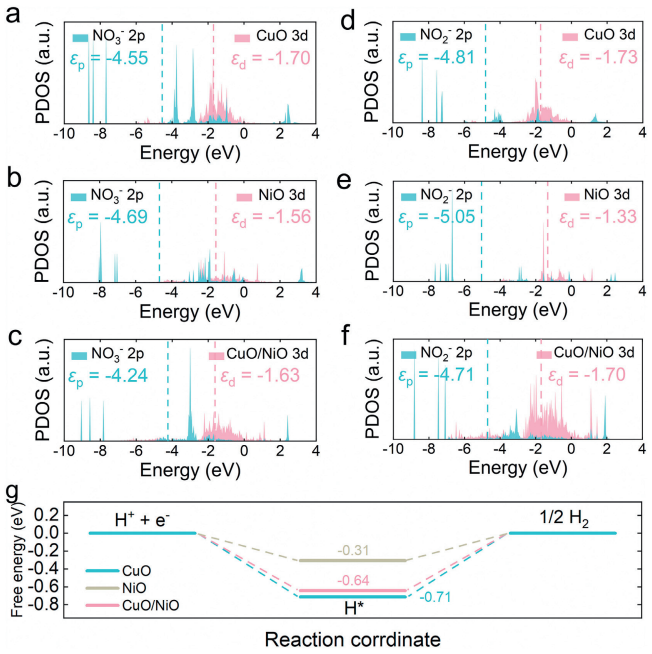

Fig. 5. PDOS of (a, d) CuO, (b, e) NiO, and (c, f) CuO/NiO with NO_3^- and NO_2^- adsorption. (g) Calculated Gibbs free energies for HER on CuO/NiO and pure CuO and NiO.

The free energy diagrams of hydrogen evolution reaction (HER) on CuO/NiO and pure CuO and NiO are investigated. As shown in Fig. 5g, the energy barrier of hydrogen evolution on CuO/NiO is calculated to be 0.64 eV, which is lower than that on CuO (0.71 eV). The result reveals the improvement of H_2O-to-H* (Volmer step) on CuO/NiO, increasing the coverage of H* on interface sites. Besides, the energy barrier of hydrogen evolution on CuO/NiO is much higher than that on NiO (0.31 eV). It is known that NiO is one of the intensively investigated semiconductors for HER. The result manifests that the generated H* in CuO/NiO cannot be easily released to generate hydrogen, but can be used as a "proton warehouse" to promote electrocatalytic reduction of NO_3^- [18,32]. The simulation results are consistent with the experimental observations and verify the enhanced H* provision of CuO/NiO for electrocatalytic reduction of NO_3^-.

Considering the removal of NO_3^- pollution in real wastewater, electrocatalytic conversion of NO_3^- to N_2 was investigated by combining CuO/NiO system and electrochlorination (Eqs. 1–4) [40,41]. As shown in Fig. 6a, when the ratio of NaCl and Na_2SO_4 is 1:4, the NH_4^+ selectivity decreases to 92.2%, and N_2 is generated during the reaction. An increase in the NaCl concentration (*i.e.*, the ratio of NaCl and Na_2SO_4 are 2:3 and 3:2) further decreases NH_4^+ selectivity (from 60.2% to 3.6%), while N_2 selectivity significantly increases (from 39.8% to 96.4%). When the ratio of NaCl and Na_2SO_4 is 4:1, the degraded NO_3^- is completely converted to N_2. Moreover, the intermediate byproducts, NO_2^- and NH_4^+, are not detected during the reaction, suggesting that NO_3^- is rapidly converted to N_2 (Fig. 6b). Furthermore, no undesired products (such as chloramines) were generated after the reaction, manifesting that NO_3^- could be efficiently transformed into N_2 in the coupling process of electrocatalytic NRA and electrochlorination (Fig. S10 in Supporting information) [34]. The residual chlorine concentration (1.1 mg/L) complied with the concentration limits specified by the World Health Organization (0.2–5.0 mg/L) [30]. In addition, the structural stability of CuO/NiO after undergoing the coupling process of electrocatalytic NRA and electrochlorination is verified by XRD measurement, demonstrating that chloride ions do not corrode the CuO/NiO electrode (Fig. S11 in Supporting infor-

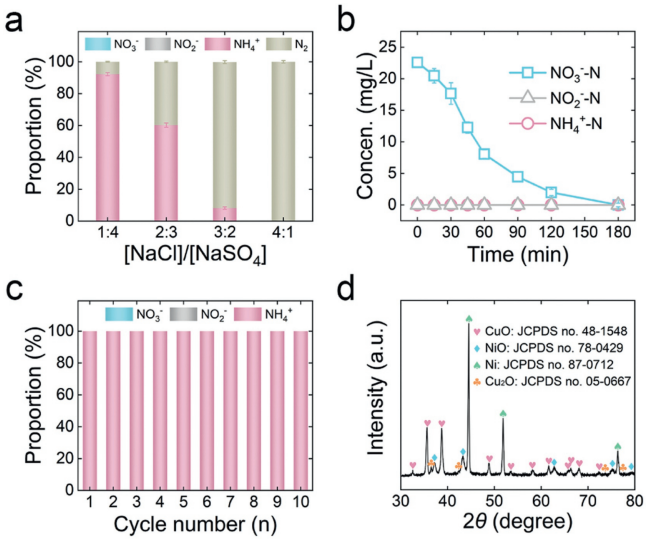

Fig. 6. (a) Effect of the molar ratio of NaCl and Na_2SO_4 on NO_3^- conversion (the total molar concentration of NaCl and Na_2SO_4 was 0.05 mol/L). (b) Time-dependent changes in the concentrations of NO_3^--N, NO_2^--N, and NH_4^+-N of CuO/NiO in the molar ratios of NaCl and Na_2SO_4 of 4:1. (c) Product distribution of electrocatalytic NO_3^- reduction by CuO/NiO in cycle tests (each test lasting 180 min). (d) XRD pattern of CuO/NiO after cycle 1 test.

mation). The experiment study on the treatment of pickle wastewater further confirmed the durability and feasibility of CuO/NiO for efficient NO_3^--N removal efficiency (92.6%) and long-term operation (Fig. S12 in Supporting information). These results demonstrate that CuO/NiO system can achieve NO_3^--NH_4^+-N_2 conversion of wastewater by combining electrocatalytic NRA and electrochlorination.

$$2Cl^- \rightarrow Cl_2 + 2e^- \quad (1)$$

$$Cl_2 + H_2O \rightarrow HClO + H^+ \ Cl^- \quad (2)$$

$$HClO \rightarrow ClO^- + H^+ \quad (3)$$

$$2NH_4^+ + 3ClO^- \rightarrow N_2 + 3H_2O + 3Cl^- + 2H^+ \quad (4)$$

To further evaluate the potential of CuO/NiO for practical application, its electrocatalytic stability evaluation was conducted by consecutive cycle tests. As shown in Fig. 6c, the NO_3^- conversion and NH_4^+ selectivity remain 100% during ten cycles of 180 min electrocatalytic NRA reaction, indicating the excellent electrocatalytic stability of CuO/NiO. Besides, the leaching of Cu and Ni during cycle tests is not detected (Fig. S13 in Supporting information). Notably, a small content of NO_2^- is detected at 120 min of cycle 1 test, the decreased content of NO_2^- is detected at 120 min of cycle 2 test, and no NO_2^- within 120 min is detected from cycle 3 to cycle 10 (Fig. S14 in Supporting information). To ascertain the origin of this increment, XRD, TEM, and XPS analysis further characterized the CuO/NiO after cycle 1 test. The XRD patterns of the post-tested CuO/NiO were presented in Fig. 6d. Except for the diffraction peaks of CuO and NiO, the additional diffraction peaks in the XRD patterns are assigned to Cu_2O (JCPDS No. 05–0667). TEM image further confirms the formation of Cu_2O, which is evident from the distinct lattice fringe of 0.151 nm corresponding to (220) plane of Cu_2O (Fig. S15a in Supporting information). XPS analysis was performed to further identify the chemical state of post-tested CuO/NiO. As shown in Fig. S15b (Supporting information), the peaks at 932.20 eV and 934.50 eV in the Cu $2p_{3/2}$ spectrum match well with Cu^+ and Cu^{2+}, respectively. Cu^{2+} is the main form of Cu species in the post-tested CuO/NiO. As shown in Fig. S15c (Supporting information), the intensity of Ni^{3+} peak of post-tested CuO/NiO increases compared to that of CuO/NiO before reaction. The XPS analysis of the post-tested CuO/NiO indicates that although partial CuO is reduced to Cu_2O, the constructed CuO/NiO heterostructure is stable during electrocatalytic NRA process, wherein electron transfers from NiO to CuO [14,23]. It is reported that Cu_2O is more beneficial than CuO for electrocatalytic NRA, which can explain the enhanced NO_3^- conversion obtained by post-tested CuO/NiO [42–44]. Dring 50 cycles tests, the NO_3^- conversion and NH_4^+ selectivity gradually decreased from 23 cycles to 29 cycles. The decline might be attributed to the reduction of partial CuO to metallic Cu during the consecutive cycle tests, which was comparatively unfavorable for electrocatalytic NRA [2,45]. The electrode was then calcined under the air atmosphere at 500 °C for 1 h. The NO_3^- conversion and NH_4^+ selectivity increased to 100% and remained almost unchanged from 30 cycles to 50 cycles. Given that coexisting ions and dissolved organics are typically present in real wastewater, the effect of these coexisting substances on electrocatalytic NRA performance is further investgated. As shown in Fig. S17 (Supporting information), the addition of CO_3^{2-} and SO_3^{2-} had no effect on the electrocatalytic NRA performance. However, the inclusion of metal ions (Fe^{2+}, Mg^{2+}, and Ca^{2+}) decreased the NO_3^- conversion, NH_4^+ selectivity, and FE. The phenomenon could be attributed to the occupation of the active sites by the metal ions [46]. Humic acid had little effect on the conversion efficiency of NO_3^- to NH_4^+, which may be due to the strong complexation between humic acid and active sites. Therefore, CuO/NiO shows practical application in nitrate control in industrial wastewater/groundwater treatment.

In this work, we demonstrate that CuO/NiO electrocatalyst can enhance mass transfer of reactants and H* provision, achieving NO_3^- conversion of 100% and NH_4^+ selectivity of 100% under NO_3^- concentration conditions (100 mg/L NO_3^-, *ca.* 22.6 mg/L NO_3^--N). The built-in electric field is spontaneously generated at CuO/NiO interface, efficiently enhancing the adsorption of reactants on heterojunction interface and hybridization between reactants and CuO/NiO, as revealed by UPS analysis and DFT calculations. The enhanced H* provision in CuO/NiO is also supported by the free energy diagram of HER. These experiments (such as combining electrocatalytic NRA and electrochlorination, stability evaluation) further show the potential of CuO/NiO in practical water applications. This work implies an effective approach for the design and manipulation of electrocatalysts to achieve electrocatalytic reduction of NO_3^- at low concentrations to NH_4^+. Further studies on the ammonia collection system are still needed [47].

Declaration of competing interest

The authors declare that they have no known competing financial interests or personal relationships that could have appeared to influence the work reported in this paper.

CRediT authorship contribution statement

Ying Chen: Conceptualization, Data curation, Formal analysis, Investigation, Methodology, Project administration, Validation, Visualization, Writing – original draft, Writing – review & editing. **Xingyuan Xia:** Conceptualization, Data curation, Formal analysis, Investigation, Methodology, Validation, Visualization, Writing – original draft. **Lei Tian:** Funding acquisition, Project administration, Software, Supervision, Validation, Writing – review &

editing. **Mengying Yin:** Data curation, Formal analysis, Methodology, Resources, Validation, Visualization. **Ling-Ling Zheng:** Investigation, Methodology, Resources, Validation. **Qian Fu:** Data curation, Methodology, Supervision, Validation, Visualization. **Daishe Wu:** Conceptualization, Project administration, Resources, Validation, Writing – review & editing. **Jian-Ping Zou:** Formal analysis, Funding acquisition, Methodology, Project administration, Writing – review & editing.

Acknowledgments

We gratefully acknowledge the financial support of the National Natural Science Foundation of China (Nos. 52170082, 51938007, 21906076, and 52300081), the Natural Science Foundation of Jiangxi Province (No. 20212ACB203008).

Supplementary materials

Supplementary material associated with this article can be found, in the online version, at doi:10.1016/j.cclet.2024.109789.

References

[1] D. Liu, L.L. Qiao, S.Y. Peng, et al., Adv. Funct. Mater. 33 (2023) 2303480.
[2] W.D. Chen, X.Y. Yang, Z.D. Chen, et al., Adv. Funct. Mater. 33 (2023) 2300512.
[3] Z. Shu, H.F. Chen, X. Liu, et al., Adv. Funct. Mater. 33 (2023) 2301493.
[4] Y.F. Fu, S. Wang, Y. Wang, et al., Angew. Chem. Int. Ed. 62 (2023) e202303327.
[5] Z.M. Song, Y. Liu, Y.Z. Zhong, et al., Adv. Mater. 34 (2022) 202204306.
[6] F.Y. Chen, Z.Y. Wu, S. Gupta, et al., Nat. Nanotechnol. 17 (2022) 759–767.
[7] W.J. Sun, H.Q. Ji, L.X. Li, et al., Angew. Chem. Int. Ed. 60 (2021) 22933–22939.
[8] Y.T. Wang, P. Zhang, X.Y. Lin, et al., Sci. China Chem. 66 (2023) 913–922.
[9] H.J. Wang, Y.A. Guo, C.J. Li, et al., ACS Appl. Mater. Interfaces 14 (2022) 34761–34769.
[10] Y.F. Gao, S. Liang, B.M. Liu, et al., Nat. Commun. 14 (2023) 2059.
[11] P. Chang, Y.H. Wang, Y.T. Wang, Y.Y. Zhu, Chem. Eng. J. 450 (2022) 137804.
[12] Y. Zhang, C.Q. Ma, X.J. Zhu, Adv. Energy Mater. 13 (2023) 2301492.
[13] T.P.Y. Taraka, A. Gautam, S.L. Jain, S. Bojja, U. Pal, J. CO_2 Util. 31 (2019) 207–214.
[14] L. Chen, H.Y. Wang, W.W. Tian, et al., Small 20 (2024) 2307252.
[15] W.X. Chen, W. Wei, F. Li, et al., Adv. Funct. Mater. 34 (2024) 2310690.
[16] L. Chen, L.G. Yue, X.Y. Wang, et al., Small 19 (2023) 2206462.
[17] B.Y. Kim, J.H. Ahn, J.W. Yoon, et al., ACS Appl. Mater. Interfaces 8 (2016) 34603–34611.
[18] Y. Feng, L. Chen, Z.Y. Yuan, et al., Inorg. Chem. Front. 10 (2023) 5225–5243.
[19] F. Zhou, G.H. Tao, J. Phys. Chem. C 127 (2023) 23180–23188.
[20] T.Y. Kou, M.P. Chen, F. Wu, et al., Nat. Commun. 11 (2020) 590.
[21] H.B. Ma, Z.W. Chen, Z.L. Wang, C.V. Singh, Q. Jiang, Adv. Sci. 9 (2022) 2105313.
[22] D. Yin, D. Chen, Y.X. Zhang, et al., Adv. Funct. Mater. 33 (2023) 2303803.
[23] Y. Xu, Y.W. Sheng, M.Z. Wang, et al., J. Mater. Chem. A 10 (2022) 16883–16890.
[24] S. Ni, H.G. Qu, H.F. Xing, et al., Chinese J. Chem. Eng. 41 (2022) 320–328.
[25] M.H. Jiang, Q. Zhu, X.M. Song, et al., Environ. Sci. Technol. 56 (2022) 10299–10307.
[26] T.L. Ren, Z. Yu, H.J. Yu, et al., Appl. Catal. B: Environ. 318 (2022) 121805.
[27] C.L. Liu, G. Zhang, W. Zhang, Z.N. Gu, G.B. Zhu, P. Natl. Acad. Sci. U. S. A. 120 (2023) e2209979120.
[28] Y. Xu, K.K. Shi, T.L. Ren, et al., Small 18 (2022) 2203335.
[29] Y. Wang, S. Shu, M. Peng, et al., Nanoscale 13 (2021) 17504.
[30] Q.A. Song, M. Li, X.S. Hou, et al., Appl. Catal. B: Environ. 317 (2022) 121721.
[31] Y. Li, J.X. Ma, Z.C. Wu, Z.W. Wang, Environ. Sci. Technol. 56 (2022) 8673–8681.
[32] J. Zhou, M. Wen, R. Huang, et al., Energy Environ. Sci. 16 (2023) 2611–2620.
[33] S.Q. Yang, X.L. Wang, D.Y. Jin, et al., Sep. Purif. Technol. 326 (2023) 124815.
[34] L. Tian, X.Y. Xia, L.J. Zhou, et al., Appl. Catal. B: Environ. 340 (2024) 123260.
[35] K. Fan, W.F. Xie, J.Z. Li, et al., Nat. Commun. 13 (2022) 7958.
[36] L. Tian, L.S. Zhang, L.L. Zheng, et al., Angew. Chem. Int. Ed. 61 (2023) e202214145.
[37] S. Zhang, M. Li, J.C. Li, Q. Song, X. Liu, Natl. Acad. Sci. U. S. A. 120 (2023) e2207080119.
[38] G.F. Chen, Y.F. Yuan, H.F. Jiang, et al., Nat. Energy 5 (2020) 605–613.
[39] W.J. Zhu, F. Yao, Q.F. Wu, et al., Energy Environ. Sci. 16 (2023) 2483.
[40] L. Tian, P. Chen, X.H. Jiang, et al., Water Res. 209 (2022) 117890.
[41] L.H. Su, K. Li, H.B. Zhang, et al., Water Res. 120 (2017) 1–11.
[42] H.B. Yin, Y. Peng, J.H. Li, Environ. Sci. Technol. 57 (2023) 3134–3144.
[43] J.J. Zhou, Y.Q. Zhu, K.Y. Wen, et al., Environ. Sci. Technol. 58 (2024) 4824–4836.
[44] J.J. Zhou, F. Pan, Q.F. Yao, et al., Appl. Catal. B: Environ. 317 (2022) 121811.
[45] T.H. Zhu, Q.S. Chen, P. Liao, et al., Small 16 (2020) 2004526.
[46] G.M. Jiang, M. Peng, L. Hu, et al., Chem. Eng. J. 435 (2022) 134853.
[47] Z.X. Liu, F. Shen, L. Shi, et al., Environ. Sci. Technol. 57 (2023) 10117–10126.